EFDA-JET-CP(06)05-28

T. Hellsten, M. Laxåback, T. Bergkvist, T. Johnson, F. Meo, F. Nguyen, C.C. Petty, M. Mantsinen, G. Matthews, J-M. Noterdaeme, , T. Tala, D. Van Eester, P. Andrew, P. Beaumont, V. Bobkov, M. Brix, J. Brzozowski, L-G. Eriksson, C. Giroud, E. Joffrin, V. Kiptily, J. Mailloux, M.-L. Mayoral, I. Monakhov, J. Ongena, R. Sartori, A. Staebler, E. Rachlew, E. Tennfors, A. Tuccillo, A. Walden, K.-D. Zastrow and JET EFDA contributors

# Fast Wave Current Drive and Direct Electron Heating in JET ITB Plasmas

# Fast Wave Current Drive and Direct Electron Heating in JET ITB Plasmas

T. Hellsten[1], M. Laxåback[1], T. Bergkvist[1], T. Johnson[1], F. Meo[2], F. Nguyen[3], C.C. Petty[4], M. Mantsinen[5], G. Matthews[6], J-M. Noterdaeme[7,8], , T. Tala[9], D. Van Eester[10], P. Andrew[6], P. Beaumont[6], V. Bobkov[7], M. Brix[7], J. Brzozowski[1], L-G. Eriksson[3], C. Giroud[6], E. Joffrin[3], V. Kiptily[6], J. Mailloux[6], M.-L. Mayoral[6], I. Monakhov[3], J. Ongena[10], R. Sartori[11], A. Staebler[7], E. Rachlew[12], E. Tennfors[1], A. Tuccillo[13], A. Walden[6], K.-D. Zastrow[6] and JET EFDA contributors*

*[1]Fusion Plasma Physics, Association EURATOM-VR, EES, KTH, Sweden,*
*[2]Association EURATOM-Risø, National Laboratory, Denmark,*
*[3]Association Euratom-CEA, CEA-Cadarache, France,*
*[4]General Atomics, San Diego,USA,*
*[5]HUT and [9]VTT, Association EURATOM-Tekes, Finland,*
*[6] Association EURATOM-UKAEA, Culham Science Centre, U.K.,*
*[7]Max-Planck IPP- EURATOM Assoziation, Garching, Germany,*
*[8]EESA Department, University of Gent, Belgium,*
*[10]LPP-ERM/KMS, Association Euratom-Belgian State, Belgium,*
*[11]EFDA CSU-Garching, Germany,*
*[12]Dept. of Physics, Association EURATOM-VR,KTH, Sweden,£*
*[13]ENEA, Association EURATOM-ENEA, Italy,*
** See annex of M. L. Watkins et al, "Overview of JET Results",*
*(Proc. 21st IAEA Fusion Energy Conference, Chengdu, China (2006)).*

Preprint of Paper to be submitted for publication in Proceedings of the
21st IAEA Fusion Energy Conference,
(Chengdu, China, 16th October - 22nd October 2006)

**ABSTRACT.**

Fast wave current drive experiments have been performed in JET plasmas with electron internal transport barriers produced with LHCD. The central plasma current was difficult to affect, even though the calculated current drive efficiency was fairly high, 0.07A per W absorbed by the electrons. The main reasons are: the strongly inductive nature of the plasma current; the interplay between the fast wave driven current and the bootstrap current, which, due to the dependence of the bootstrap current on the poloidal magnetic field, decreases the bootstrap current as the driven current increases; and parasitic absorption of the waves that decreased the power absorbed by the electrons. The measured difference in the central current density for co and counter current drive is larger than the response expected from current diffusion calculations, suggesting a faster current diffusion than that given by neoclassical resistivity. Effective direct electron heating, comparable to the indirect electron heating with H-minority heating, is found for the dipole phasing of the antennas without producing a significant fast ion pressure and with low impurity content in the divertor plasma even though the single pass damping is only a few percent. For the ±90o phasings producing current drive, with a similar single pass damping, strong degradation of the heating is observed with strong increases in the BeII and CIV line intensities in the divertor. The degradation depends on the phasing of the antennas and increases with reduced single pass damping, consistent with RF-power being lost by dissipation of rectified RF-sheath potentials at the antennas and walls. Asymmetries in direct electron heating, lost power, production of impurities, fast ions and gamma-rays are seen for co and counter current drive that are consistent with differences in the absorption on residual 3He ions due to the RF-induced pinch.

## 1. INTRODUCTION

Experiments with Fast Wave Current Drive (FWCD), and heating have been carried out in JET Internal Transport Barrier (ITB) ITB, discharges with strongly reversed magnetic shear [1]. For such plasmas the control of the current profile is important to maximize performance and avoid instabilities. The advantage of using waves in the ion cyclotron range of frequencies is the unrestrained access to high-density plasmas. Direct electron heating with fast magnetosonic waves by transit time magnetic pumping and electron Landau damping, TTMP/ELD, has the advantage over indirect heating via cyclotron heated high-energy ions of a prompt heating without increasing the fast ion pressure, and it can also provide a more peaked heating profile than minority heating with broad high-energy ion orbits. The strong localisation of the driven current near the magnetic axis makes fast wave current drive a potential tool for controlling the central current in tokamak plasmas. Because of the weak single pass damping by TTMP/ELD in present day experiments it is important to avoid parasitic absorption, in particular ion cyclotron absorption, which can damp a large fraction of the power and thereby substantially degrade the current drive efficiency. FWCD experiments in the higher harmonic ion cyclotron frequency range have earlier been carried out with positive magnetic shear in L-mode [2, 3] and in H-mode [4], and in plasmas with negative magnetic shear [5].

## 2. EXPERIMENTAL RESULTS

In order to maximize the current drive efficiency and increase the electron damping, and at the same time modify the current profile in the transport barrier, hot low density ITB plasmas, $n_e \approx 1.2\times10^{19}m^{-3}$, with strongly reversed magnetic shear, close to current hole, were created using nearly 3s of 2–2.5MW of Lower Hybrid Current Drive, LHCD, preheating at 3.7GHz. The LHCD preheat was switched off when around 13MW of NBI and up to 6MW of ICRF power were applied, Fig.1. To avoid disruptions the NBI was stepped down when the barrier expanded as $q_{min}$ reached 2. Even though strict precautions were taken to avoid $^3$He in the plasma, the presence of high-energy $^3$He ions was seen. During the application of NBI- and RF-heating, the plasma current, 2MA, and the toroidal vacuum field, 3.45T at R = 2.96m, were kept constant. The RF power was applied at a frequency of 37MHz, placing the hydrogen resonance outside the plasma at the low-field side, the deuterium resonance inside the plasma on the far high-field side and the resonance of any residual $^3$He ions near the magnetic axis. The four strap A2 antennas with beryllium Faraday screens were used: with 180° phasing (dipole phasing) producing a symmetric spectrum peaked at $n_\phi \approx \pm25$; and with ±90° phasing producing asymmetric toroidal mode spectra peaked at $n_\phi \approx \pm15$, driving currents anti-parallel (+) and parallel (–) to the ohmic current, respectively.

The effects on the central current by FWCD and heating were studied by comparing similar discharges obtained with different heating powers at different ICRH phasings such as the tripple of Pulse No's: 60664 (–90°), 60663 (+90°) and 60667 (dipole), Fig.2. A small but clear difference in the central current density could be detected with the Faraday rotation polarimeter, Fig.3. Because of the similar electron temperatures the difference is not expected to be caused by different current diffusion rates. Even though the calculated current drive efficiency in terms of ampere per watt absorbed by the electrons was fairly high for the ±90° phasings, 0.07A/W, it was difficult to strongly affect the central plasma current.

Direct electron heating by fast magnetosonic waves using dipole spectra was proven to be an effective method to heat electrons in high-temperature ITB plasmas, Fig.4, even for a single pass damping of only a few percent. The heating efficiency was comparable to H-minority heating with +90° at 51MHz (6% H in D). The heating in FWCD experiments with the ±90° antenna phasings were, for similar single pass damping as for the dipole, strongly degraded by parasitic losses and with a heating efficiency of about half that of the dipole. Evidence of the strong degradation in heating for the ±90° phasings was obtained by: (i) observing that similar plasmas were obtained at different levels of coupled RF-power for the different phasings, Fig.2; (ii) comparing heating at the same power, Fig.4; (iii) comparing the integrated power delivered by the heating systems to the sum of the integrated radiated power (from bolometry) and the integrated power delivered to the divertor (from thermocouple measurements), Table 1. The difference in heating efficiency between different phasings is clearly seen when comparing the triple of discharges shown in Fig.2. that had very similar electron temperatures and densities during $5 < t < 6$s. The average coupled power between $5 < t < 5.5$s, just before the modulation, was 5.0MW for Pulse No:

60663 with $+90^{o}$ phasing, 6.2MW for Pulse No: 60664 with $-90^{o}$ phasing and 3.0MW for Pulse No: 60667 with dipole phasing. Similar direct electron heating profiles were also seen by modulating the RF-power. From this we conclude that the heating efficiency is reduced to about 50% for the $-90^{o}$ phasing and to about 60% for the $+90^{o}$ compared to the dipole phasing. In Fig.4 we compare the electron temperature and diamagnetic energy for a discharge, Pulse No: 58682 ($+90^{o}$, 51MHz, 4.2MW) with minority hydrogen heating to discharges with direct electron heating Pulse No's: 60673 (3.4MW, dipole), 60675 (5.6MW, $+90^{o}$) and 60676 (5.7MW, $-90^{o}$). The larger diamagnetic energy content of Pulse No: 58682 compared to Pulse No:60673 is due to the fast H ions.

Evidence of power not absorbed and transferred to the plasma was obtained by comparing the energy delivered by the heating systems to the sum of the radiated energy (from bolometry) and the energy delivered to the divertor (from thermocouple measurements, see Table 1. This was best seen for discharges dominated by ICRH, such as in Pulse No: 58680 without NBI where 33MJ (63%) of the total delivered heating energy of 52MJ came from the RF system. 18MJ (34% of the total heating) was accounted for by the thermocouplers; 18MJ (34%) was measured by the bolometers; 17MJ (32%) was not accounted for. The lost energy corresponds to 51% of the injected RF energy and is well above the error bars for the method, ±12% for this discharge as derived from the normal levels of accuracy of the experimental signals. Likely causes of the lost RF power are losses of RF-heated high-energy ions intercepted by the wall or the limiters and energy dissipated in rectified RF-sheaths at the antennas and the wall. For discharges with dominating NBI heating as were the case in most of these discharges the losses were in general within the error bars. Thus, a large fraction of the delivered RF power was not transferred to the bulk plasma. The fraction of power absorbed and transferred to the bulk plasma increased with single pass damping and depended on the phasing.

Observations supporting that the losses are primarily caused by the presence of rectified RF-sheath potentials came from the large differences in performance, in BeII and CIV line radiation intensities between discharges heated with the dipole and $\pm 90^{o}$ phasings. Large intensity spikes in the BeII and CIV line radiation at the edge were seen for the $\pm 90^{o}$ phasings, similar to those earlier observed for monopole phasing and interpreted as arcs [6], Fig.6. Spikes did not appear for the dipole phasing and the average level of radiation was also much lower, consistent with the lower rectified RF-sheath potentials for this phasing.

## 3. MODELLING OF HEATING AND CURRENT DRIVE

The magnetosonic waves are expected to be damped directly by TTMP/ELD and by cyclotron damping on $^{3}$He and C impurity ions and on D majority ions. The waves can also be absorbed indirectly through mode conversion to kinetic Alfvén waves near the high-field side edge. Complete modelling of the driven current requires calculations of the power absorbed by TTMP/ELD, the driven steady state current and the response of the plasma current to the current drive. The triple of Pulse No's: 60663 with $+90^{o}$ phasing, 60664 with $-90^{o}$ phasing and 60667 with dipole phasing is used for comparison with numerical modelling. The evolution of the discharges during the first 2s after the

onset of ICRH and NBI heating were quite similar and the experimental profiles for Pulse No's: 60663 and 60664 could be regarded as identical for this period. Pulse No: 60667 had initially a little lower density and higher electron temperature. Around t = 5.5s, before the power modulation periods, all discharges had similar plasmas despite the different coupled ICRH powers of 4.4MW forœhe $+90^{o}$, 5.8MW for $-90^{o}$ and 2.3MW for the dipole, Fig.2. The modulation for Pulse No: 60663 did not start until t = 6.5s, after the NBI step down, and for comparison with the measured direct electron damping we therefore use data from the very similar Pulse No: 660665.

The driven steady state currents shown in Fig.7 (a) are calculated with the LION code [7–9] for a reconstructed experimental equilibrium using as input data the power absorbed directly on the electrons as measured with the modulation technique. The power is normalised so that the calculated power absorbed on electrons by TTMP/ELD agrees with that measured. For these discharges 9-10% of the total power is absorbed on electrons in the centre of the plasma, which according to LION corresponds to a total electron absorption in the plasma of around 17%. The power absorbed by TTMP/ELD was for $+90^{o}$ 0.8MW and for $-90^{o}$ 1MW, yielding driven currents of –55kA and 70kA respectively. The corresponding current drive efficiencies are of the order 0.07A/W per watt absorbed on the electrons.

The effect of the current drive on the evolution of the central plasma current was simulated with the JETTO code [10]. To clearly quantify the effects of the current drive the same discharge, Pulse No: 60664, was simulated with both co and counter current drive as well as without current drive for reference. The simulation was started at t = 4.7s, well before the power modulation at t = 5.5s, and lasted until the onset of the ITB around 2.6s later. The resulting plasma current profiles due to RF, NBI and bootstrap currents and poloidal flux diffusion are shown in Fig.7. The total plasma current in the centre changes only with a small fraction of the RF driven current. After 2.6s the differences in current density inside r/a = 0.3 compared to the reference simulation without current drive are of the order $+10kA/m^2$ to $+30kA/m^2$ for co current drive and $-10kA/m^2$ to $-15kA/m^2$ for counter current. Right at the magnetic axis the difference in current density between the two current drive simulations is about $130kA/m^2$. This should be compared to the driven current densities calculated with LION, which are around $+80kA/m^2$ and $-70kA/m^2$, respectively at r/a = 0.3 and increases to about $+400kA/m^2$ and $-300kA/m^2$ at the magnetic axis. Owing to the inductive nature of the plasma current the application of fast wave current drive results in an immediate change in the local electric field such that the net current density is left unchanged. An effect of the driven current is not seen until this back EMF diffuses away. This effect is expected to be symmetric for the two phasings for the same amount of power absorbed by TTMP/ELD. In addition, the RF driven current is also partly compensated for by an opposite change in the bootstrap current due to the dependence of the bootstrap current on the poloidal field, which is an asymmetric effect, and is the reason of the difference in response for co and counter current drive. Halfway into the simulation, at t = 6s, the total difference in the calculated central current density is only between $10kA/m^2$ and $40kA/m^2$ between co and counter current drive simulations. Measurements of the central current density in the corresponding $\pm 90^{o}$

discharges using the Faraday rotation polarimeter, however, showed a difference in current density of around 100kA/m$^2$ at this time, Fig.2. This indicates that poloidal flux diffusion takes place on a faster time scale than that given by neoclassical resistivity.

In the absence of accurate data of the 3He concentration and the fraction of the power absorbed in the centre of the plasma estimates of the maximum power lost by fast ions intercepted by the wall were done by simulating the RF-heating and fast particle losses with the SELFO code [11, 12]. For the Pulse No's: 60663, 60664 and 60667 the maximum possible losses of RF power with fast $^3$He ions hitting the wall was estimated by scanning the 3He impurity content from 0.01% to 0.5% of the background D density, using the experimental profiles just before the start of the modulation at 5.5s and assuming that 2.9MW was absorbed in the plasma. The maximum losses reached 30% for the dipole and about 20% for the $\pm 90^o$ phasings, the losses peaked at a lower concentration for $+90^o$ compared to $-90^o$, Fig.8. Thus the simulations with the SELFO code showed that the losses of heated $^3$He ions were insufficient to explain the observed imbalances in integrated power. The experimentally observed imbalance was in general larger for $-90^o$ than for $+90^o$, whereas the RF power absorbed directly on electrons was equal or larger for $-90^o$ in similar plasmas. This is qualitatively consistent with a better heating at stronger single pass damping for an inward RF-pinch with $+90^o$, accumulating residual 3He ions in the centre, compared to heating with $-90^o$ having a weaker single pass damping with an inverted RF-pinch.

The measured difference in fast-energy content of about 0.1MJ between the +90° and $-90^o$ phasings is according to SELFO for these simulations inconsistent with a steady-state 3He concentration much above 0.1%. At that concentration the calculated fast-energy content with the +90° phasing was around 0.13MJ and with the $-90^o$ and dipole phasings about 0.02MJ. The RF power was in the simulations predominantly partitioned between the electrons and the $^3$He, Fig.8. Less than one percent of the RF power was absorbed by cyclotron damping on majority D and impurity C ions. For the $-90^o$ and dipole phasings the RF power was roughly equally partitioned between electrons and $^3$He ions for a $^3$He concentration of 0.4%. For the $+90^o$ phasing they were equally partitioned already around a $^3$He concentration of 0.05% due to the RF-induced inward pinch. At 0.1% $^3$He concentration the power absorbed by electrons was about 35% with the $+90^o$ phasing, 80% with the $-90^o$ phasing and 70% with the dipole phasing.

In order to correlate the heating efficiency with the single pass damping we have to estimate the single pass damping in the presence of non-thermal $^3$He ions. This is done by first calculating the single pass damping coefficients at t = 5.5s. For thermal plasmas the damping was 0.4% for $^3$He damping at a concentration of 0.1% $^3$He, and 2.3% for electron damping with the $\pm 90^o$ phasings. The corresponding coefficients for the dipole phasing were 0.2% for $^3$He damping and 1.8% for electron damping. For non-thermal steady state plasmas the total single pass damping was then estimated to be about 3–7% by comparing the power partition calculated with the SELFO code to the thermal power partition. The higher value is for $+90^o$ and is caused by the RF-induced pinch and the lower value is for $-90^o$ (inverted RF-induced pinch) and the dipole.

## CONCLUSIONS

Fast wave electron current drive experiments have been performed in JET ITB plasmas. The current drive was found to be degraded by strong parasitic absorption in rectified RF-sheaths due to the low single pass damping. It was difficult to strongly modify the central plasma current, even though the calculated current drive efficiency in terms of ampere per watt absorbed by the electrons was fairly high for the $\pm 90^{o}$ phasings, 0.07A/W. The main reasons are: (i) the strongly inductive nature of the plasma current due to the high electric conductivity at the high electron temperatures; (ii) the interplay between the fast wave driven current and the bootstrap current, which, due to the dependence of the bootstrap current on the poloidal magnetic field, decreases the bootstrap current as the driven current increases; and (iii) parasitic absorption of the waves that decreased the power absorbed by the electrons.

The measured difference in central current density for co and counter current drive is larger than the modelled response on the plasma current from the current drive, but smaller than the calculated steady state current drive. This suggests a faster current penetration time than that given by the neoclassical resistivity.

Direct electron heating by fast magnetosonic waves using dipole spectra has been proven to be an effective method to heat electrons, comparable to H-minority heating, in these JET ITB plasmas with strongly reversed magnetic shear. Observations supporting that the losses are primarily caused by the presence of rectified RF-sheath potentials come from the differences in BeII line radiation intensities and the large differences in performance between the dipole and the $\pm 90^{o}$ phasings. In addition, the calculated maximum losses of fast ions are for all phasings smaller than the observed imbalance in energy. FWCD in this frequency range is more promising for ITER and future reactors since the single pass damping in these plasmas will be much higher due to their larger size, higher densities and higher temperatures.

## REFERENCES


[1]. Hellsten, T., et al., Nuclear Fusion **45** (2005) 706-720.

[2]. Equipe Tore Supra and Saoutic, B., et al., Plasma Physics and Controlled Fusion **36** (1994) B123.

[3]. Petty, C.C., et al., Nuclear Fusion **35** (1995) 773.

[4]. Petty, C.C., et al., Nuclear Fusion **39** (1999) 1421.

[5]. Prater, R., et al., in Fusion Energy 1996 (Proc. 16th Int. Conf. Montreal, 1996) Vo. 3, IAEA, Vienna (1997) 243.

[6]. Heikkinen, J., et al., Experiments on ICRF coupling with different phasings, 2004 31st EPS on Controlled Fusion Plasma Physics, London.

[7]. Villard, L. et al., Computer Physics Reports **4** (1986) 95.

[8]. Villard, L. et al., Nuclear Fusion **35** (1995) 1173.

[9]. Hellsten, T., and Eriksson, L. G., "An analysis of trapped particle effects on fast wave current profiles", in Proc. IAEA Technical Committee Meeting on Fast Wave Current Drive in Reactor Scale Tokamaks, Arles, France, ed. D. Moreau, A. Bécoulet and Y. Peysson (1991).

[10]. Tala, T. J., et al., Nuclear Fusion **40** (2000) 1635.

[11]. Hedin, J., Hellsten, T., and Carlsson, J., 1998 in Proc. of Joint Varennna-Lausanne Workshop "Theory of Fusion Plasmas" pp. 467, Varenna ISBN 88-7794-167-7.

[12]. Laxåback, M., et al., Nucl. Fusion **45** (2005) 1510.

| No | phase | (%) RF power accounted for | (MJ) Total heating energy | (%) RF heating energy | (%) Energy to bolo-meter | (%) Energy to thermo-couplers | (%) Energy lost | $Z_{eff}$ | (MW) Average RF power | Direct electron damping, r/a < 0.5 Early/late | (keV) $T_e$ Early/late |
|---|---|---|---|---|---|---|---|---|---|---|---|
| 58679 | $-90^o$ | 58±31 | 119 | 30 | 29 | 59 | 13 | 4.2 | 4.4 | n.a. | 8.3 / 5.9 |
| 58680[1] | $+90^o$ | 49±12 | 52 | 63 | 34 | 34 | 32 | 3.7 | 4.0 | n.a. | 3.8 / 3.9 |
| 58681 | $+90^o$ | 65±32 | 120 | 30 | 28 | 62 | 10 | 4.2 | 4.5 | n.a. | 8.3 / 6.2 |
| 58682[2] | $+90^o$ | 83±32 | 108 | 32 | 25 | 70 | 6 | 3.8 | 4.2 | n.a. | 8.1 / 8.1 |
| 58684 | $+90^o$ | 62±32 | 154 | 30 | 27 | 62 | 12 | 4.1 | 5.7 | n.a. | 8.2 / 7.6 |
| 60661 | $-90^o$ | 50±39 | 109 | 24 | 33 | 55 | 12 | 4.2 | 4.3 | 0.11 / 0.11 | 6.2 / 6.4 |
| 60662 | $-90^o$ | 50±32 | 117 | 29 | 30 | 55 | 14 | 4.3 | 5.5 | 0.11 / 0.10 | 6.9 / 6.6 |
| 60663 | $+90^o$ | 82±33 | 93 | 29 | 38 | 57 | 5 | 4.5 | 4.4 | 0.12[3] / 0.10 | 6.8 / 5.7 |
| 60664 | $-90^o$ | 59±28 | 110 | 32 | 30 | 57 | 13 | 4.5 | 5.8 | 0.10[4] / 0.05[4] | 8.2 / 5.4 |
| 60665 | $+90^o$ | 77±32 | 103 | 30 | 34 | 59 | 7 | 4.3 | 5.1 | 0.09 / 0.07 | 7.5 / 6.3 |
| 60667 | $180^o$ | 44±68 | 90 | 16 | 29 | 63 | 9 | 3.8 | 2.3 | 0.20[5] / | 8.5 / 5.9 |
| 60668 | $-90^o$ | 57±42 | 112 | 24 | 29 | 61 | 10 | 4.2 | 4.4 | n.a. | 8.0 / 7.5 |
| 60673 | $180^o$ | 59±40 | 85 | 25 | 28 | 62 | 10 | 3.9 | 3.4 | 0. 23/0.13 | 8.7/5.7 |
| 60674 | $180^o$ | 53±46 | 103 | 22 | 30 | 60 | 10 | 4.0 | 3.7 | n.a. | 7.2/7.7 |
| 60675 | $+90^o$ | 56±34 | 122 | 28 | 29 | 59 | 12 | 4.2 | 5.6 | 0.13 /n.a. | 7.6 / 8.3 |
| 60676 | $-90^o$ | 52±28 | 110 | 32 | 29 | 56 | 15 | 4.5 | 5.7 | 0.28 / 0.05 | 7.0 / 5.8 |

CP060528T1

[1] *No NBI.*
[2] *Power at a frequency of 51MHz, heating of H-minority.*
[3] *Early phase around t =46s and late phase at t=49s, first modulation phase occurred after beam step down.*
[4] *Within r/a < 0.3.*
[5] *Within r/a < 0.4.*
[6] *At the peak of the expanded barrier.*

*Table 1*

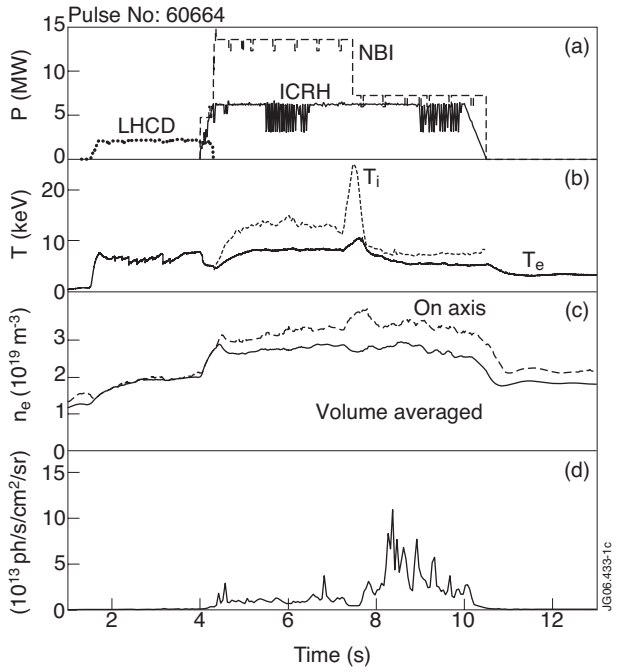


*Figure 1: Time traces for Pulse No: 60664. (a) NBI, ICRF and LHCD power, (b) central electron, $T_e$, and ion, $T_i$, temperature, (c) electron density, ne, and (d) BeII line radiation intensity.*

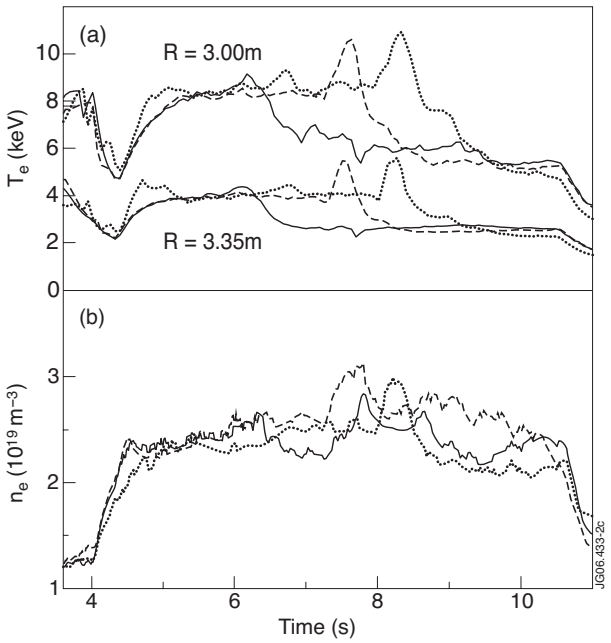


*Figure 2: Comparison of (a) electron temperatures at R =3.00m and R = 3.35m and (b) central electron density for Pulse No's: 60663 (full), 60664 (dashed) and 60667 (dotted). The NBI step down took place at t = 6.13s for Pulse No: 60663, at t = 7.48s for Pulse No: 60664 and at t = 7.14s for Pulse No: 60667.*

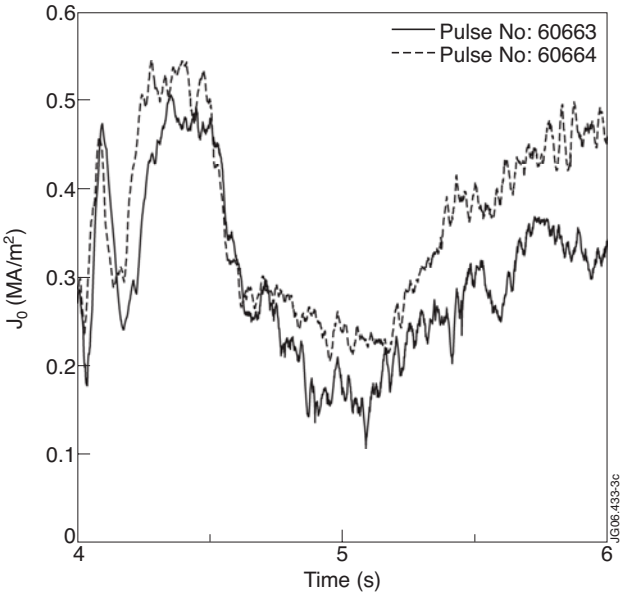


*Figure 3: Central current density derived from Faraday rotation.*

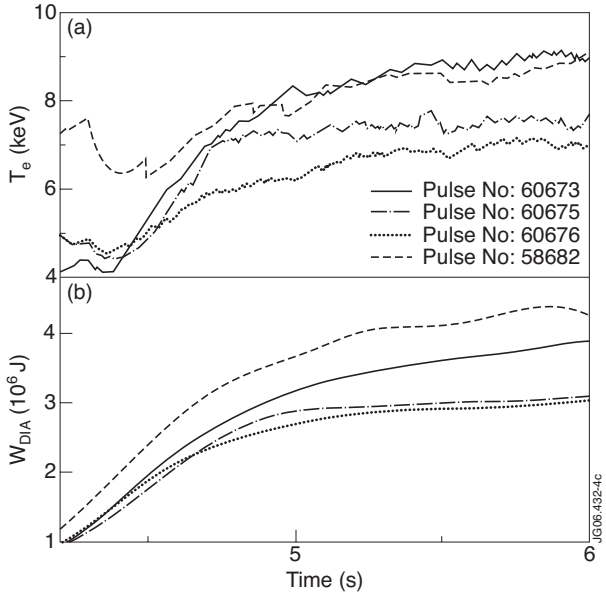


*Figure 4: (a) Central electron temperatures and b) diamagnetic energy, for Pulse No: 58682 with 4.2MW +90$^o$ 51MHz, Pulse No: 60673 with 3.4MW dipole, Pulse No: 60675 with 5.6MW +90$^o$ and 60676 with 5.7MW –90$^o$*

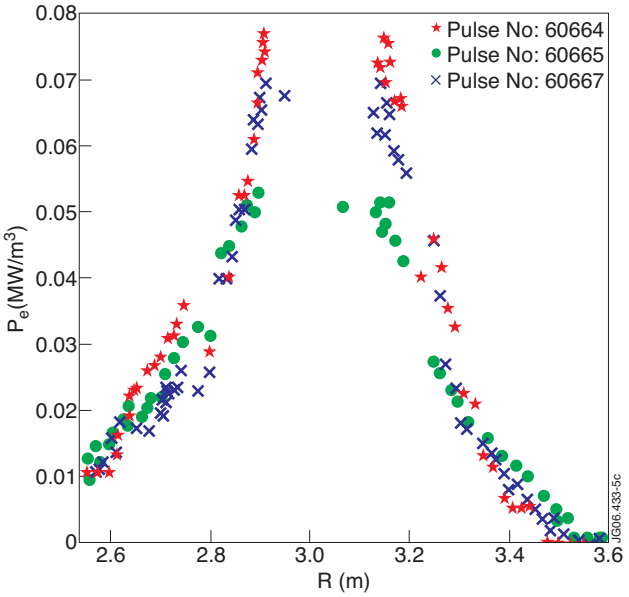


*Figure 5: Power deposition by direct electron heating obtained with modulation between 5.5 and 6.5s for Pulse No: 60664 with 5.8MW $-90^o$, Pulse No: 60665 with 5.1MW $+90^o$ and Pulse No: 60667 with 2.3MW dipole.*

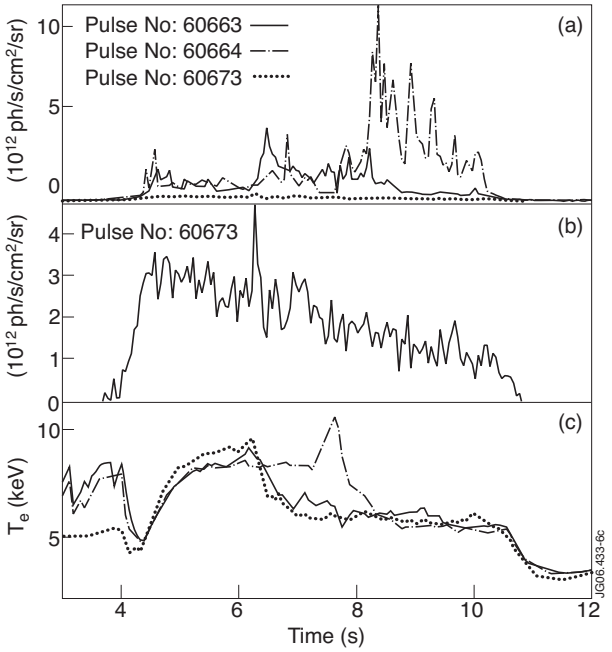


*Figure 6: (a) and (b) BeII line intensity through a sight line passing the inner divertor,(b) with a higher resolution. (c) electron temperature.*

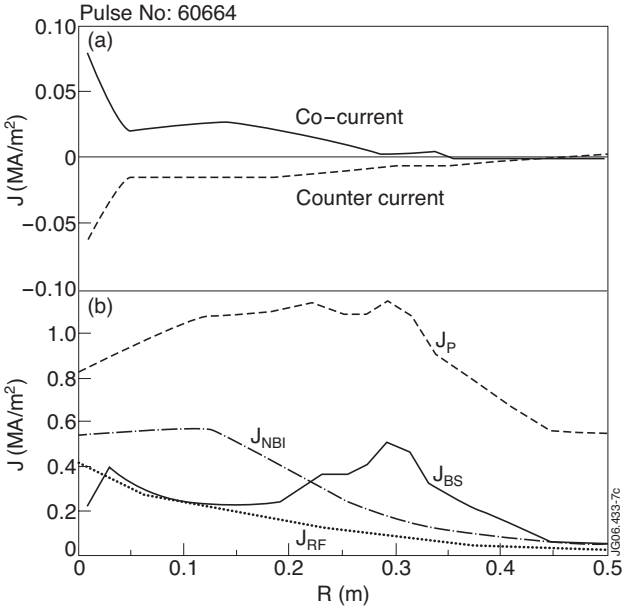


*Figure 7: (a) Calculated change of the current density at t = 2.6s after onset of the RF. (b) Total plasma current density, RF- and NBI-driven current densities and bootstrap current densities at the same time for $-90^o$.*

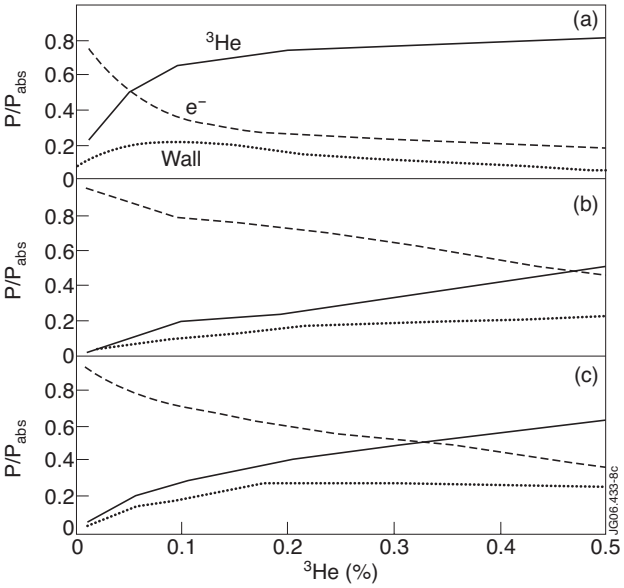


*Figure 8: Calculated steady state power partition between electron and $^3$He absorption, and wall losses by $^3$He versus $^3$He concentration assuming $P_{abs}$ = 2.9MW absorbed in the plasma for (a) $+90°$ (b) $-90^o$ and (c) dipole phasing.*